PERGAMON

International Journal of Heat and Mass Transfer 44 (2001) 4483–4492

International Journal of HEAT and MASS TRANSFER

www.elsevier.com/locate/ijhmt

A phenomenological approach to correcting DNB-type critical heat flux for non-uniform axial power shapes

Dae-Hyun Hwang *, Cheol Park, Sung-Quun Zee

Korea Atomic Energy Research Institute, Advanced Reactor Devlopment Division, P.O. Box 105, Yusong, Daejon 305-600, South Korea

Received 8 August 2000; received in revised form 19 February 2001

Abstract

A theoretically based correction-factor model is proposed for the prediction of the DNB-type critical heat flux (CHF) in a boiling channel with non-uniform axial power shapes. The basic formulation of the correction factor is devised from the mass balance equation in the bubble layer, which was employed by Weisman and his coworkers for the prediction of CHF at low quality conditions. The key parameters representing the influence of the upstream heat flux profile are revealed as the bubble layer thickness, the mixture velocity of the bubble layer directed parallel to the heated wall, and the lateral mass velocity from core to bubble layer caused by the turbulence. The validity of the model is examined on the CHF data with various axial power shapes for round tubes and rod bundles. In view of the result so far achieved, the proposed model reveals reasonable accuracy in comparison with existing correction-factor models. © 2001 Published by Elsevier Science Ltd.

1. Introduction

One of the most important requirements in the design of water-cooled nuclear reactor is to avoid the occurrence of critical heat flux (CHF) at which the boiling heat transfer coefficient in the core begins to deteriorate and finally results in fuel failure. The design criteria for nuclear reactors specify that they must be operated at a certain percentage below the CHF at all times and locations in order to maintain the cladding temperature of the fuel element at safe values. The prediction of CHF has been, in most cases, based on the empirical correlation. For PWR fuel assemblies the local parameter correlation requires the local thermal-hydraulic conditions usually calculated by a subchannel analysis code. The cross-sectional averaged fluid conditions of the subchannel, however, are not sufficient for determining CHF, especially for the cases of non-uniform axial heat flux distributions. Many investigators have studied on the influence of upstream history of heat flux variation to the CHF. In terms of the upstream history effect, two different approaches have been considered as the limiting cases. The 'local conditions' hypothesis assumes that there is a unique relationship between the CHF and the local thermal-hydraulic conditions, and consequently there is no memory effect. In the 'overall power' hypothesis, on the other hand, it is assumed that the total power which can be fed into the tube with non-uniform heating will be the same as that for a uniformly heated tube of the same heated length with the same inlet conditions. Thus the CHF is totally influenced by the upstream heat flux distribution. However, in view of some experimental investigations such as the DeBortoli's test [1], it revealed that the two approaches are inadequate in general. It means that the local critical heat flux may be affected to some extent by the upstream history of heat flux variations. Consequently, various correction-factor models have been suggested to take into account the upstream history effect. Bowring [2] introduced a parameter Y, which is defined as the ratio of the length-averaged heat flux to the local heat flux. He observed that the upstream history effect decreases as mass flux increases. Reddy et al. [3] confirmed this observation through the evaluation of CHF data for rod bundles with non-uniform axial power shapes. Tong [4] devised a correction-factor model on the basis of the heat balance of the superheated liquid layer that is

* Corresponding author. Tel.: +82-42-468-8730; fax: +82-42-864-1089.

E-mail address: dhhwang@kaeri.re.kr (D.-H. Hwang).

0017-9310/01/$ - see front matter © 2001 Published by Elsevier Science Ltd.
PII: S0017-9310(01)00092-8

Nomenclature

d_{he}/d_{hy}	heated/hydraulic equivalent diameter (m)
d_g	distance from last grid to CHF location (m)
F	correction factor for non-uniform heat flux profiles
G	mass flux (kg/m^2/s)
h	specific enthalpy (kJ/kg)
j	superficial velocity (m/s)
$\dot{m}$	mass flow rate (kg/s)
P	pressure (bar)
q''	heat flux (kW/m^2)
R	channel radius (m)
S_L	slip ratio in bubble layer region
T	temperature (°C)
Y	Bowring's Y-factor $(\equiv \int_0^z q''(z')\,dz'/\{q''(z)\,z\})$
z	distance from channel inlet (m)

Greek symbols

α	void fraction
χ	quality
δ_b	bubble layer thickness (m)
Φ_b	fraction of total heat flux effective in generating vapor
ρ	density (kg/m^3)

Subscript

1	core region
2	bubble layer region
3	from core region to bubble layer region
b	boiling or bubble layer
f, g	saturated liquid and saturated vapor, respectively
m	mixture property

spread underneath a highly viscous bubble layer along the heated surface. He assumed the superheated liquid layer would have a unique value of enthalpy at the CHF location independent of the axial power distributions. However, the model coefficient, C_T, was determined empirically since the heat transfer rate from the superheated liquid layer to the bubble layer was not examined. The correction factor goes to the value of Bowring's Y-factor as C_T goes to zero. Groeneveld et al. [5] adopted a correction factor expressed by the boiling-length-averaged heat flux for their CHF-lookup-table method. This model implies that the overall power hypothesis is valid over the boiling region. Smolin [6] proposed a relaxation length model in that the relaxation length was empirically determined as a function of hydraulic diameter only. In view of the functional form of the correction-factor model, the relaxation length is corresponding to the inverse of C_T in the Tong's model.

Recently, theoretical approaches to examine the governing mechanism of CHF have been attempted in various ways, and some of them are successfully applied to the round tubes and rod bundles at flow boiling conditions [7]. In the subcooled and low-quality regions, Weisman and Pei [8] found that their bubble coalescence model was capable of predicting CHF in round tubes with varying axial heat fluxes without any correction or modification. Subsequently, Weisman and Ying [9] showed that this approach is also applicable to rod bundles with uniform and sinusoidally varying heat fluxes for relatively long heated channels. Yang and Weisman [10] conducted CHF tests for a relatively short sinusoidally heated tube with R-113 to show whether the 'local conditions' hypothesis would hold with a sharper variation in heat flux. To explain the effect of sharply varying heat fluxes on CHF, they exhibit the complete energy balance on the bubbly layer that contains the enthalpy derivative term. Based on these findings, we devised a theoretically based correction-factor model to explain the upstream history effect.

2. Model development

2.1. Formulation of the correction factor

In this study we devised a correction-factor model on the basis of the bubble-crowding model suggested by Weisman and Pei [8]. The physical model of the transport phenomena in the vicinity of the CHF is illustrated in Fig. 1. The basic formulation of the correction-factor is derived from the mass balance in bubble layer and the

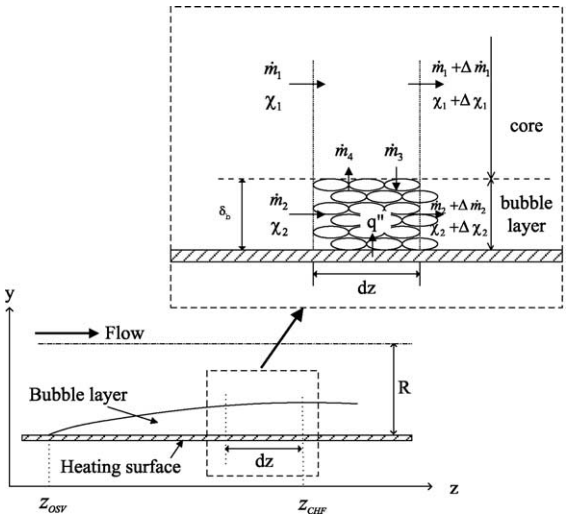

Fig. 1. Proposed physical model at CHF location.

energy balance in the boiling channel. The total mass balance in the bubble layer is written as

$$\Delta\dot{m}_2 = \dot{m}_3 - \dot{m}_4. \tag{1}$$

A mass balance of liquid in the bubble layer yields

$$\dot{m}_2(1-\chi_2)+\dot{m}_3(1-\chi_1) = (\dot{m}_2+\Delta\dot{m}_2)\{1-(\chi_2+\Delta\chi_2)\} + \dot{m}_4(1-\chi_2)+\frac{q''_b(2\pi R)\Delta z}{h_{fg}}. \tag{2}$$

By combining these mass balances, when second-order terms are ignored, we obtain

$$\dot{m}_3(\chi_2-\chi_1) = \frac{q''_b(2\pi R)\Delta z}{h_{fg}} - \dot{m}_2\Delta\chi_2. \tag{3}$$

Since $\dot{m}_2 \equiv G_2(2\pi R)\delta_b\zeta$ and $\dot{m}_3 \equiv G_3(2\pi R)\zeta'\Delta z$, Eq. (3) can be rewritten as

$$G_3\zeta'(\chi_2-\chi_1) = \frac{q''(z)\Phi_b}{h_{fg}} - G_2\delta_b\zeta\frac{d\chi_2}{dz}, \tag{4}$$

where $\zeta = 1-\delta_b/(2R)$, $\zeta' = 1-\delta_b/R$, and Φ_b is the fraction of heat input used for vapor generation. Weisman and Pei neglected the last term of Eq. (4) in their CHF prediction model. In this study, we account for the axial convection of enthalpy in the bubble layer region that is regarded as a key parameter governing the upstream history effects. The following assumption can be made from the heat balance relationship along the channel:

$$\frac{d\chi_1}{dz} \cong \frac{d\bar{\chi}}{dz} = \frac{4q''(z)}{Gd_{he}h_{fg}}. \tag{5}$$

Then Eq. (4) can be rewritten as

$$\frac{d}{dz}(\chi_2-\chi_1) + C(z)(\chi_2-\chi_1) = A(z)\ q''(z), \tag{6}$$

where

$$A(z) \equiv \frac{4}{Gd_{he}h_{fg}}\left(\frac{Gd_{he}}{4G_2(z)\ \delta_b(z)\ \zeta(z)}\Phi_b(z) - 1\right), \tag{7}$$

$$C(z) \equiv \frac{G_3(z)\ \zeta'(z)}{G_2(z)\ \delta_b(z)\ \zeta(z)}. \tag{8}$$

Since the net vapor generation will be initiated from the onset of significant void (OSV) location, we adopted a boundary condition for the local quality as

$$\chi_2-\chi_1 = 0, \quad \text{at} \quad z = z_{OSV}. \tag{9}$$

For an arbitrary axial power shape, the solution of the above first-order ordinary differential equation can be obtained as

$$(\chi_2-\chi_1)_{NU} = e^{-\bar{C}_{NU}(z)\ (z-z_{OSV})}\ \bar{A}_{NU}(z) \times \int_{z_{OSV}}^{z} q''(z')\ e^{\bar{C}_{NU}(z')(z'-z_{OSV})}\,dz', \tag{10}$$

where

$$\bar{C}_{NU}(z) = \frac{1}{(z-z_{OSV})}\int_{z_{OSV}}^{z} C(z')\,dz' \tag{11}$$

and

$$\bar{A}_{NU}(z) \equiv \frac{\int_{z_{OSV}}^{z} A(z')\ q''(z')\ e^{\bar{c}_{NU}(z')(z'-z_{OSV})}dz'}{\int_{z_{OSV}}^{z} q''(z')\ e^{\bar{c}_{NU}(z')(z'-z_{OSV})}\,dz'}. \tag{12}$$

For a uniform axial power shape the solution of Eq. (6) becomes

$$(\chi_2-\chi_1)_{EU} = \frac{\bar{A}_{EU}(z)}{\bar{C}_{EU}(z)}\ q''_{EU}(z)\left[1-e^{-\bar{C}_{EU}(z)(z-z_{OSV})}\right], \tag{13}$$

where

$$\bar{A}_{EU}(z) \equiv \frac{\int_{z_{OSV}}^{z} A(z')\ \ e^{\bar{c}_{EU}(z')(z'-z_{OSV})}\,dz'}{\int_{z_{OSV}}^{z} e^{\bar{c}_{EU}(z')(z'-z_{OSV})}\,dz'}. \tag{14}$$

The subscript 'EU' means the 'equivalent uniform' heat flux distribution that results in the same local thermal-hydraulic conditions with those for the corresponding non-uniform heat flux distribution. Thus the following relationship is held between the equivalent uniform heat flux and the local heat flux

$$q''_{EU}(z) = q''(z)\ Y(z). \tag{15}$$

If we assume that the CHF is a local phenomenon, then the local quality in the bubble layer, χ_2, at the CHF location should have a unique value which is independent of the upstream heat flux profiles. According to the definition of the correction factor, the CHF for an arbitrary axial power shape is calculated by

$$q''_{CHF}(z_{CHF}) = q''_{CHF,EU}(z_{CHF})/F, \tag{16}$$

where $q''_{CHF,EU}(z_{CHF})$ is the CHF for uniform axial power shape under the local thermal hydraulic conditions determined from the corresponding actual heat flux distribution. Thus from Eqs. (10) and (13), by assuming $\bar{C}_{NU}(z) \approx \bar{C}_{EU}(z)$, we can obtain the basic formulation of the correction factor as

$$F = \frac{K_1(z_{CHF})\ K_2(z_{CHF})C_N}{q''(z_{CHF})\ \{1-e^{-K_2(z_{CHF})C_N\ (z_{CHF}-z_{OSV})}\}} \times \int_{z_{OSV}}^{z_{CHF}} q''(z)\ e^{-K_2(z)(z_{CHF}-z)}\ dz, \tag{17}$$

where

$$K_1(z) \equiv \bar{A}_{NU}(z)/\bar{A}_{EU}(z), \tag{18}$$

$$K_2(z) \equiv \bar{C}(z)/C_N \tag{19}$$

and

$$C_N = \left[\frac{G_3(z')}{G_2(z')\ \delta_b(z')}\right]_{z'=z_{CHF}}. \quad (20)$$

The functional form of the proposed correction-factor model is compared with various existing models in Table 1. The parameter C of the proposed model is expressed as a function of the turbulent lateral velocity from core to bubble layer (G_3), the mixture velocity in bubble layer parallel to the heated wall (G_2), and the bubble layer thickness at CHF location (δ_b). Tong's model and Smolin's model adopted empirically determined parameters, while the Groeneveld's model is equivalent to the Bowring's Y-factor over the boiling length region.

2.2. Constitutive equations

The lateral mass flux caused by turbulence from core to bubble layer can be expressed as [8]

$$G_3 = G\psi i_b. \quad (21)$$

The turbulent intensity at the interface of bubble layer and core (i_b), and the parameter related to the probability distribution of fluctuating velocity (ψ) are calculated from the Weisman and Pei model.

The mass velocity of the two-phase mixture in the bubble layer is calculated by

$$G_2 = \{\alpha_2\rho_g S_L + (1-\alpha_2)\rho_f\}u_2, \quad (22)$$

where S_L is the slip ratio in the bubble layer. Since many studies on the bubble behavior near the heated wall still do not come to agreement in general, S_L is arbitrarily determined in this study on the basis of a parametric analysis. The liquid velocity in the bubble layer, u_2, is evaluated by the Karman velocity distribution model for turbulent flow through a tube, which can be represented by the three-layer distribution of liquid velocity as a function of distance from the wall. The liquid velocity in the bubble layer is calculated at the distance of $\delta_b/2$ from the wall.

The axial variation of bubble layer thickness is calculated by Jiji and Clark model [11] that is given as

$$\delta_{b0}(z) = 2.716\times10^{-3}\times\frac{(q''_{loc})^{1.256}\ (z-z_{OSV})^{0.534}}{(T_{sat}-T_{in})^{1.163}G^{0.504}}. \quad (23)$$

It is assumed that the radius of the boiling channel restricts the maximum thickness of the bubble layer. For a uniform axial heat flux distribution, the maximum thickness appears always at the channel exit. In this case we assume that the bubble layer thickness grows up to the channel radius at the location of the onset of annular flow (OAF) condition.

The OSV location is predicted by the Saha and Zuber model [12], and the fraction of the total heat flux effective to the vapor generation is calculated by the Shah model [13]. The overall procedure for the calculation of the proposed correction factor is described in Appendix A.

3. Model assessment

3.1. Parametric trends

Fig. 2 illustrates the behavior of the upstream history effect using experimental data obtained in a rectangular channel with a hot patch [1]. This figure shows a clear dependency of the upstream effect on the local thermodynamic quality. In addition, the experimental data demonstrate the inadequacy of the 'local conditions' and the 'overall power' hypotheses as general statements. The parametric trend of the proposed model is compared with the experimentally determined correction factors in the figure. The proposed model shows relatively good prediction accuracy at low quality region,

Table 1
Comparison of various CHF correction models for non-uniform axial heat flux distribution

Model	Parameter C	Correction factor
Proposed model	$C = K_2\left.\frac{G_3}{G_2\delta_b}\right\|_{z=z_C}$	$F = \frac{K_1 C\int_{z_{OSV}}^{z_C} q''e^{-C(z_C-z)}dz}{q''_{loc}\{1-e^{-C(z_C-z_{OSV})}\}}$
Tong [4]	$C = 5.906\times\frac{(1-\chi_C)^{4.31}}{(G/1356)^{0.478}}$	$F = \frac{C\int_{z_{ONB}}^{z_C} q''e^{-C(z_C-z)}dz}{q''_{loc}\{1-e^{-C(z_C-z_{ONB})}\}}$
Smolin [6]	$C = \frac{1}{40d_{hy}}$	$F = \frac{C\int_0^{z_C} q''e^{-C(z_C-z)}dz}{q''_{loc}}$
Groeneveld [5]	$C = 0$	$F = \frac{\int_{z_b}^{z_C} q''(z)dz}{q''_{loc}(z_C-z_b)}$

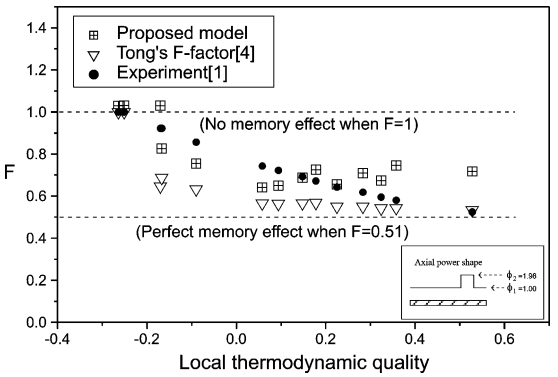

Fig. 2. Analysis of parametric behavior for a rectangular channel.

while tends to underestimate the upstream history effect at high quality conditions.

For a given channel geometry, various local quality conditions can be obtained by changing thermal power input, inlet temperature, or the mass velocity. Fig. 3 shows the parametric trend of the proposed model with respect to the local quality that is calculated by changing the inlet subcooling at a fixed heat flux condition. A cosine-shaped axial power distribution is used in this calculation. In the proposed model, the parameter C decreases mainly due to the increase of bubble layer thickness as shown in Fig. 3, and results in the increase of the correction factor. When the mass flux increases at fixed inlet conditions, the parameter C increases mainly due to the decrease of the bubble layer thickness and results in the decrease of the upstream history effect as shown in Fig. 4. If the channel hydraulic diameter increases, then G_3 decreases due to the reduction of turbulent intensity and results in the increase of the correction factor as shown in Fig. 5. Smolin's relaxation length model and Groeneveld's boiling-length-average model show similar parametric behavior, while Tong's F-factor model does not indicate any diameter effects.

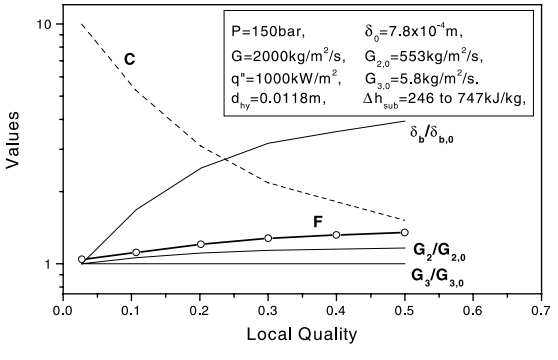

Fig. 3. Parametric behavior of the proposed model for quality at fixed heat flux condition.

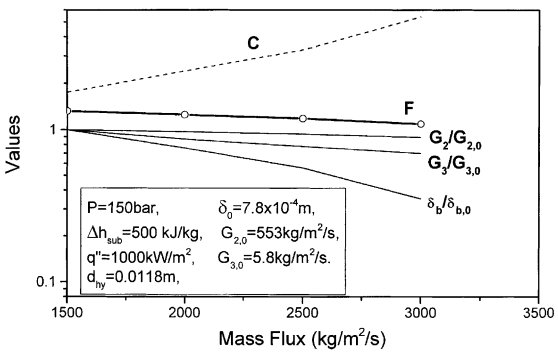

Fig. 4. Parametric behavior of the proposed model for mass flux at fixed inlet condition.

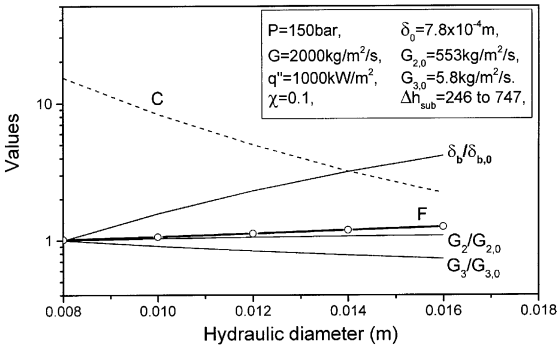

Fig. 5. Parametric behavior of the proposed model for channel hydraulic diameter at fixed local condition.

3.2. Analysis of single-channel CHF data

The performance of the proposed correction factor model is assessed for round tubes with various axial power shapes [14–19] including inlet peaks, middle peaks, outlet peaks, and a step change of heat fluxes. According to the physical basis of the proposed model we selected CHF data for relatively low critical qualities at which the corresponding void fractions are less than 0.8. All these 308 data points were obtained at the pressure ranges from 68 to 180 bars, mass flux ranges from 373 to 4069 kg/m^2/s, and the critical thermodynamic quality ranges from −0.14 to 0.38. The CHF location is determined at which the predicted-to-measured CHF ratio (P/M) is the minimum for all axial levels along the channel. The CHF values are calculated by the CHF lookup table method [20] with a correction factor for the non-uniform axial power shape. Fig. 6 shows the minimum CHFR locations calculated by the proposed model for round tubes with various axial power shapes. For the step-peak power distribution, the minimum CHFR always occurs at the end of the largest power step. The maximum deviation between the predicted and

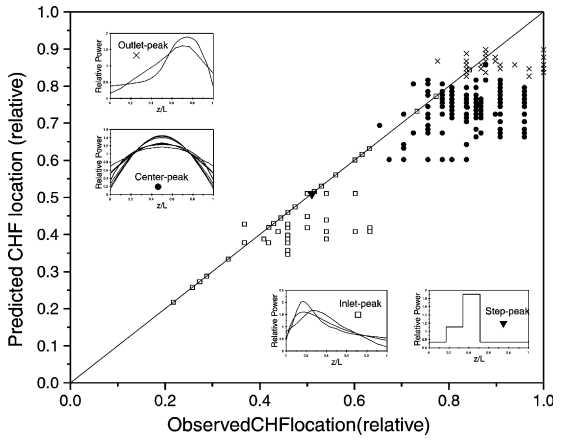

Fig. 6. Comparison of observed and predicted CHF locations for round tubes calculated by the proposed model.

observed CHF locations is calculated at about 30%. The analysis results of P/M are summarized in Table 2 with respect to the profile of axial power distribution. The P/M is calculated by increasing the channel power until it reaches the calculated critical power. As presented in the table, the mean value of P/M calculated without the correction factor tends to decrease as the axial peaking position moves toward the outlet of the channel. Considering the reliability of the CHF lookup table method for round tubes with uniform axial heat flux conditions, it reveals that the upstream history effect for the bottom-peaked heat flux profile is stronger than that for the top-peaked profile. The mean values of F calculated by the proposed model reveals decreasing trend as the axial peaking moves downstream of the channel. It means the upstream history effects are compensated adequately by the proposed model in the average sense. For the data assessed in this study, the performance of the proposed model turns out compatible to the Tong's F-factor model.

3.3. Analysis of rod-bundle CHF data

CHF data from two kinds of 5×5 square-arrayed rod bundles [21] are employed to evaluate the applicability of the proposed model. The geometry and experimental ranges of the data are representative of the pressurized water reactor conditions. Except the axial heat flux distribution, the two test bundles are geometrically identical as presented in Table 3. The validity of the proposed model is examined by the following two steps. Firstly, a local parameter CHF correlation is developed using the test bundle data for axially uniform heat flux distribution (TS-161). Secondly, this correlation is applied to the non-uniformly heated test bundle (TS-164) with various correction factors.

The local thermal-hydraulic conditions inside the test bundle are calculated by the subchannel analysis code MATRA [22] that is a modified version of COBRA-IV-I code. Referring to the previous study [23], the basic form of the local parameter CHF correlation is selected as

$$q''_{\mathrm{CHF}} = f(P, G, d, d_{\mathrm{g}}) - g(P)\ G\ \chi. \tag{24}$$

The correlation coefficients for the thermal-hydraulic parameters such as P, G, and χ are determined through a non-linear least square fitting of experimental data for TS-161 which result in

$$\begin{aligned} f(P, G, d_{\mathrm{he}}, d_{\mathrm{g}}) = {} & 2.913 \times 10^{3} + 3.126 \times 10^{-1} G \\ & - 5.476P - 5.422 \times 10^{4} d_{\mathrm{he}} \\ & - 7.956 \times 10^{2} d_{\mathrm{g}}, \end{aligned} \tag{25}$$

$$g(P) = -3.523 + 7.479 \times 10^{-2} P - 2.756 \times 10^{-4} P^{2}. \tag{26}$$

For 70 CHF data points of TS-161, the above correlation yields the mean and the standard deviation of P/M as 1.00 and 0.049, respectively.

Table 2
Results of data analysis for round tubes with various axial power shapes

Axial power shape	References	Number of data	Without F	With F calculated by			
				Proposed model	Tong	Groeneveld	Smolin
Inlet-peak	[14,17,18]	54	1.063/0.170[a]	1.011/0.154[a] 1.099[b]	0.964/0.113 1.179	0.890/0.123 1.291	1.250/0.363 1.249
Center-peak	[14–17]	199	1.007/0.075	0.978/0.076 1.086	0.979/0.075 1.230	0.989/0.065 1.218	1.173/0.184 1.285
Outlet-peak	[14,17]	42	0.849/0.049	0.906/0.054 1.077	0.884/0.062 1.071	0.838/0.060 1.147	1.548/0.292 1.015
Step-peak	[19]	13	0.739/0.040	0.844/0.048 0.877	0.972/0.059 0.761	0.740/0.039 0.999	1.801/0.097 0.410

[a] (Average of P/M)/(standard deviation of P/M).
[b] Average of F values.

Table 3
Information of CHF test bundles

	TS-161	TS-164
Axial power shape	Uniform	Cosine
Pressure (bar)	103–167	103–167
Mass velocity (kg/m^2/s)	1298–4801	1329–4793
Quality	0.04–0.30	−0.02–0.29
Data points	70	64
Rod array	5×5 square-lattice	
Rod diameter/ pitch	9.5/12.6 mm	
Heated length	4.27 m	
Grid spacing	559 mm	

This correlation is applied to TS-164 with various correction-factor models. The P/M flux ratio is calculated at the axial location where the predicted CHF ratio is a minimum along the channel. The void fractions at CHF locations calculated by Saha and Zuber model [12] range from 0.05 to 0.75. It reveals that the upstream history effect is about 15% in the average sense, as shown in Fig. 7. The proposed model reveals good prediction capability in comparison with various existing models. The influence of slip ratio on the proposed model is examined for TS-164 rod bundle. It reveals that the mean of P/M changes within 3% as the slip ratio varies from 0.5 to 2.0. Since the influence is not significant and, in addition, the slip ratio is close to unity at the relatively high pressures and velocities, we used $S_L = 1.0$ in this study.

3.4. Evaluation of K_1 and K_2

The equations of K_1 and K_2 employed in the proposed model are somewhat complicated in comparison with existing correction-factor models. In order to simplify the proposed model, we evaluate K_1 and K_2 for various rod bundles. The CHF data for eighteen square-lattice test bundles has been collected from open literature [21] that contains 704 data points from five different axial power shapes as plotted in Fig. 8. The parametric ranges of the data are as follows; pressure from 100 to 168 bars, mass flux from 1320 to 5100 kg/m^2/s, local quality up to 28%, heated length from 2.44 to 4.27 m, rod diameter from 9.5 to 12.7 mm, and rod pitch from 12.6 to 16.7 mm. The local thermal hydraulic conditions for the test bundles are calculated by the MATRA code.

As expressed in Eq. (17), K_1 directly affects the magnitude of the correction factor while K_2 influence the weighting function of heat flux in the proposed model. For the data collected in this study, it reveals that the values of K_1 approximately lie between 0.95 and 1.0 as shown in Fig. 9. On the other hand, the K_2 values tend to increase as the mass flux increases as plotted in Fig. 10. The best-fit line of K_2 is obtained as

$$K_2 = 0.466 + 0.067\left(\frac{G}{1000}\right) \tag{27}$$

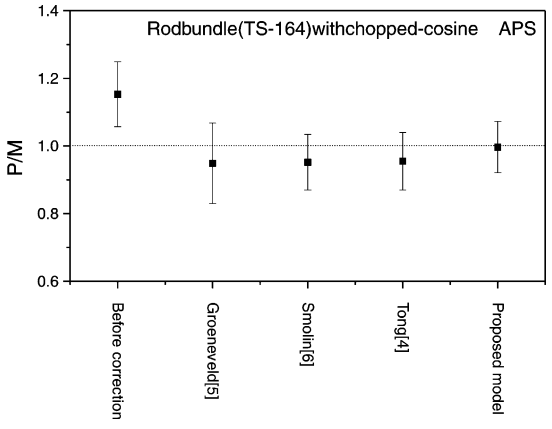

Fig. 7. Comparison of various correction-factor models for TS-164.

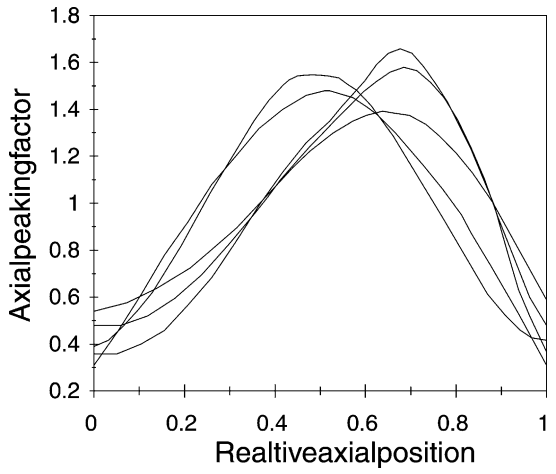

Fig. 8. Five different axial power shapes of rod bundles.

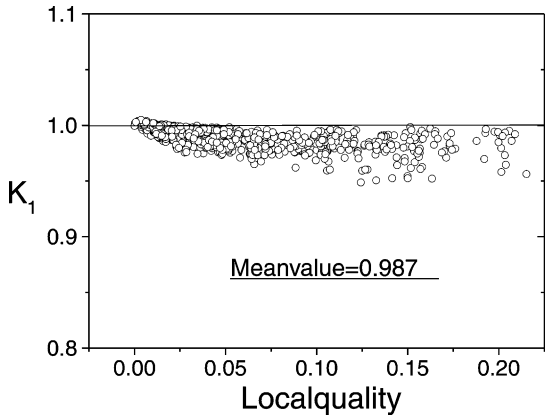

Fig. 9. Model parameter K_1 for various rod bundles.

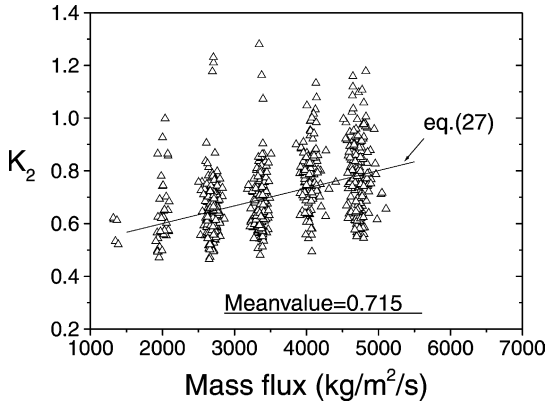

Fig. 10. Model parameter K_2 for various rod bundles.

We applied various models of K_1 and K_2 to the analysis of TS 164 with the local parameter correlation of Eq. (24). As summarized in Table 4, it reveals that Eqs. (18) and (19) can be replaced by constant values of 0.987 and 0.715 with negligible deviation of P/M statistic. For the 704 CHF data points of rod bundles, it reveals that the maximum deviation of the two correction factors is less than 3.1% as shown in Fig. 11.

Table 4
Influence of K_1 and K_2 on the correction factor

K_1	K_2	P/M statistics for TS 164 with Eq. (24)	
		Mean	Standard deviation
Eq. (18)	Eq. (19)	0.998	0.106
0.987	0.715	1.003	0.107
0.987	Eq. (27)	0.999	0.110

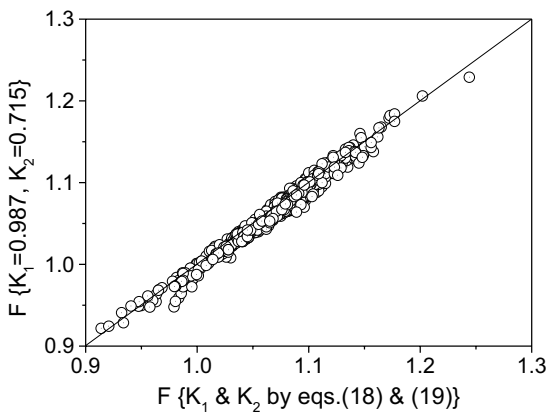

Fig. 11. Comparison of correction factors according to K_1 and K_2 models.

4. Conclusion

A correction-factor model of CHF for axially non-uniform heat flux distributions is devised on the basis of the bubble crowding and vapor removal limit model. The validity of the proposed model is examined for CHF data in a rectangular channel, round tubes, and rod bundles with various axial power shapes. As a result, it is found that the proposed model adequately explains the upstream history effect without any empirical constant derived from the CHF data for non-uniform axial power shapes. Comparing to the existing correction-factor models, the proposed model reveals reasonable parametric trends and prediction accuracy for the experimental data considered in this study. In addition, it is found that the complexity of the proposed model can be significantly reduced by replacing the complicated functions of K_1 and K_2 with constant values.

Acknowledgements

This study has been carried out under the R&D program sponsored by the Ministry of Science and Technology of Korea.

Appendix A. Calculation procedure of the proposed model

(1) Operating conditions, test section geometry, and thermodynamic properties:

$$P, G, \Delta h_{\mathrm{sub}}, q'', \mathrm{L}, d_{\mathrm{he}}, z_{\mathrm{CHF}}, \rho, h, \sigma, \mu, k, c_p.$$

(2) Calculate OSV location and Φ_{b}:
Saha and Zuber [12]

$$z_{\mathrm{OSV}} = \frac{G d_{\mathrm{he}} h_{\mathrm{fg}}}{4Y(z_{\mathrm{OSV}})q''(z_{\mathrm{OSV}})}(\chi_{\mathrm{eN}} - \chi_{\mathrm{in}}), \tag{A.1}$$

where

$$\chi_{eN} = -0.0022\frac{q''c_p d_{hy}}{h_{fg}k} \quad \text{for} \quad \frac{Gc_p d_{hy}}{k} < 70{,}000, \tag{A.2}$$

$$\chi_{eN} = -154\frac{q''}{h_{fg}G} \quad \text{for otherwise.} \tag{A.3}$$

Shah [13]:

$$\Phi_b(z) = 1 - \frac{H_{1\phi}\{T_w(z) - T_L(z)\}}{q''(z)}, \tag{A.4}$$

where

$$H_{1\phi} = 0.023\left(\frac{Gd_{hy}}{\mu}\right)^{0.8}\left(\frac{c_p\mu}{k}\right)^{0.4}\frac{k}{d_{he}}, \tag{A.5}$$

$$T_w(z) = T_L(z) + \frac{\left(230\sqrt{\frac{q''(z)}{(Gh_{fg})}} - 1\right)\{T_{sat} - T_L(z)\} + q''(z)/H_{1\phi}}{230\sqrt{q''(z)/(Gh_{fg})}}. \tag{A.6}$$

(3) Calculate parameters for bubble layer at CHF location:

Bubble layer thickness by Jiji and Clark [11]

$$\delta_b(z) = \frac{\delta_{max}}{\delta_{b0}(z_{max})}\ \delta_{b0}(z), \tag{A.7}$$

where

$$\delta_{max} = R, \tag{A.8}$$

$$z_{max} = \min\left\{z_{OAF}, \delta_{b0}^{-1}(R)\right\} \tag{A.9}$$

and $\delta_{b0}(z)$ from Eq. (23).

Average mass velocity of the bubble layer;

$$G_2 = \left\{\alpha_2\rho_g S_L + (1-\alpha_2)\rho_f\right\}\ u_2, \tag{A.10}$$

where

$$S_L = 1.0. \tag{A.11}$$

$$\alpha_2(z) = \min\left\{\alpha_c \times \frac{\bar{\alpha}(z)}{\bar{\alpha}(z_{CHF})}, \alpha_c\right\}, \quad \alpha_c = 0.82. \tag{A.12}$$

$$u_2 = U^+\sqrt{\tau_w/\rho}, \tag{A.13}$$

$$U^+ = y^+ \quad \text{for } y^+ < 5, \tag{A.14}$$

$$U^+ = 5\ln(y^+) - 3.05 \quad \text{for } 5 \leqslant y^+ < 30, \tag{A.15}$$

$$U^+ = 2.5\ln(y^+) + 5.5 \quad \text{for } y^+ \geqslant 30, \tag{A.16}$$

$$y^+ = \frac{\rho}{\mu}\left\{\frac{\delta_b(z)}{2}\right\}\sqrt{\frac{\tau_w}{\rho}}, \tag{A.17}$$

$$\tau_w = 0.023Re^{-0.2}\frac{G^2}{\rho}. \tag{A.18}$$

Mass velocity from core to bubble layer region by Weisman and Pei [8]

$$G_3 = G\psi i_b, \tag{A.19}$$

where

$$i_b = 0.790\ \mathrm{Re}^{-0.1}\left(\frac{D_b}{d_{hy}}\right)^{0.6}\left\{1 + a\frac{\Delta\rho}{\rho_g}\right\}, \tag{A.20}$$

$$D_b = 0.015\sqrt{\frac{\sigma\ d_{hy}}{\tau_w}}, \tag{A.21}$$

$$a = 0.135 \quad \text{for } G < 2694.4\ \mathrm{kg/m^2/s}, \tag{A.22}$$

$$a = 0.135(G/2694.4)^{-0.3} \quad \text{for otherwise.} \tag{A.23}$$

$$\psi = \frac{1}{\sqrt{2\pi}}\mathrm{e}^{-(v_{1L}/\sigma_{v'})^2/2} - \frac{1}{2}\left(\frac{v_{1L}}{\sigma_{v'}}\right)\ \mathrm{erfc}\left(\frac{v_{1L}}{\sigma_{v'}\sqrt{2}}\right), \tag{A.24}$$

$$\sigma_{v'} = i_b\ G/\bar{\rho}, \tag{A.25}$$

$$v_{1L}(z) = \frac{q''(z)\Phi_b(z)}{\rho_g h_{fg}}. \tag{A.26}$$

(4) Calculate K_1(z) and K_2(z) by Eqs. (18) and (19), or constant values.
(5) Calculate C_N by Eq. (20).
(6) Calculate the correction factor by numerical integration of Eq. (17).

References

[1] R.A. DeBortoli, S.J. Green, B.W. LeTourneau, M. Troy, A. Weiss, Forced-convection heat transfer burnout studies for water in rectangular channels and round tubes at pressures above 500 psia, WAPD-188, Westinghouse, 1958.

[2] R.W. Bowring, A new mixed flow cluster dryout correlation for pressures in the range 0.6–15.5 MN/m^2 (90–2250 psia) – for use in a transient blowdown code, I. Mech. E. (1977) 175–182.

[3] D.G. Reddy, C.F. Fighetti, M. Merilo, Prediction of critical heat flux in PWR fuel assemblies with non-uniform axial heat flux distribution, in: Proceedings of the Seventh International Heat Transfer Conference, Munich, 1982, pp. 333–338.

[4] L.S. Tong, Boiling Crisis and Critical Heat Flux, TID-25887, Westinghouse, 1972.

[5] D.C. Groeneveld, S.C. Cheng, T. Doan, 1986 AECL-UO critical heat flux lookup table, Heat Transfer Eng. 7 (1986) 46–62.
[6] V.N. Smolin, V.K. Polyakov, Coolant boiling crisis in rod assemblies, in: Proceedings of the Sixth International Heat Transfer Conference, Toronto, 1978, pp. 47–52.
[7] J. Weisman, The current status of theoretically based approaches to the prediction of the critical heat flux in flow boiling, Nucl. Technol. 99 (1992) 1–21.
[8] J. Weisman, B.S. Pei, Prediction of critical heat flux in flow boiling at low qualities, Int. J. Heat Mass transfer 26 (1983) 1463–1477.
[9] J. Weisma, S.H. Ying, A theoretically based critical heat flux prediction for rod bundles at PWR condition, Nucl. Eng. Design 85 (1985) 239–250.
[10] J.Y. Yang, J. Weisman, An examination of the local conditions hypothesis in subcooled and low quality CHF, in: Proceedings of the Fifth International Topical Conference on Nuclear Reactor Thermal Hydraulics (NURETH-5), Salt Lake City, 1992, pp. 691–698.
[11] L.M. Jiji, J.A. Clark, Bubble boundary layer and temperature profiles for forced convection boiling in channel flow, ASME paper 62-WA-141, 1962.
[12] P. Saha, N. Zuber, Point of net vapor generation and vapor void fraction in subcooled boiling, in: Proceedings of the Fifth International Heat Transfer Conference, Tokyo, 1974, pp. 175–179.
[13] M.M. Shah, A general correlation for heat transfer during subcooled boiling in pipes and annuli, ASHRAE Trans. 83 (1977) 202–217.
[14] H.S. Swenson, J.R. Carver, C.R. Kakarala, Influence of axial heat flux distribution on departure from nucleate boiling in water cooled tube, ASME paper 62-WA-297, 1962.
[15] D.H. Lee, J.D. Obertelli, An experimental investigation of forced convection burnout in high pressure water: Part II, preliminary results for round tubes with non-uniform axial heat flux distribution, AEEW-R309, UKAEA, 1963.
[16] D.H. Lee, An experimental investigation of forced convection burnout in high pressure water: Part III, long tubes with uniform and non-uniform axial heating, AEEW-R355, UKAEA, 1965.
[17] D.H. Lee, An experimental investigation of forced convection burnout in high pressure water: Part IV, large diameter tubes at about 1600 psia, AEEW-R479, UKAEA, 1966.
[18] K.M. Becker, P. Askeljung, S. Hedberg, B. Soderquist, U. Kahlbom, An experimental investigation of the influence of axial heat flux distributions on post dryout heat transfer for flow of water in vertical tubes, KTH-NEL-54, Royal Institute of Technology, 1992.
[19] B.A. Zenkevich, Y.A. Kalinin, C.V. Remizov, V.I. Subbotin, Effect of non-uniform axial heat flux distribution in a tube on heat transfer crisis, FEI-150, IPPE, 1969.
[20] D.C. Groeneveld, L.K.H. Leung, P.L. Kirillov, V.P. Bobkov, I.P. Smogalev, V.N. Vinogradov, X.C. Huang, E. Royer, The 1995 look-up table for critical heat flux in tubes, Nucl. Eng. Design 163 (1996) 1–23.
[21] C.F. Fighetti, D.G. Reddy, Parametric study of CHF data, EPRI-NP-2609, vol. 3 Pt. 1, Columbia University, 1982.
[22] Y.J. Yoo, D.H. Hwang, D.S. Sohn, Development of a subchannel analysis code MATRA applicable to PWR and ALWRs, J. Korean Nucl. Soc. 31 (1999) 314–327.
[23] D.H. Hwang, Y.J. Yoo, J.R. Park, Y.J. Kim, Evaluation of the thermal margin in a KOFA-loaded core by a multi-channel analysis methodology, J. Korean Nucl. Soc. 27 (1995) 518–531.